

Toward optimal X-ray flux utilization in breast CT

Jakob H. Jørgensen¹, Per Christian Hansen¹, Emil Y. Sidky², Ingrid S. Reiser², and Xiaochuan Pan²

Abstract—A realistic computer-simulation of a breast computed tomography (CT) system and subject is constructed. The model is used to investigate the optimal number of views for the scan given a fixed total X-ray fluence. The reconstruction algorithm is based on accurate solution to a constrained, TV-minimization problem, which has received much interest recently for sparse-view CT data.

I. INTRODUCTION

Dose reduction has been a primary concern in diagnostic computed tomography (CT) in recent years [1]. Interest in low intensity X-ray CT is also motivated by the potential to employ CT for screening, where a large fraction of the population will be exposed to radiation dose and the majority of subjects will be asymptomatic. This abstract examines the screening application of breast CT; we simulate breast CT projection data and perform image reconstruction based on constrained, total-variation (TV) minimization. The specific question of interest is: given a fixed, total X-ray flux, what is the optimal number of views to capture in the CT scan? As the total flux is fixed, more views implies less photons per view, resulting in a higher noise level per view. On the other hand, fewer views may not provide enough sampling to recover the underlying object function. The optimal balance of these two effects will depend on the imaged subject and the imaging task. For this reason, we have focused on the breast CT application as a case study, which also has received much attention in the literature [2]–[4].

From the perspective of non-contrast CT, the breast has essentially four gray levels corresponding to: skin, fat, fibro-glandular or malignant tissue, and calcification. In designing the CT system, physical properties of the subject that are important are the complexity of the fibro-glandular tissue, which could be the limiting factor in determining the minimum number of views in the scan, and micro-calcifications and tumor spiculations, which challenge the resolution of the system.

The image reconstruction algorithm, investigated here, is based on accurate solution of constrained, TV-minimization. Constrained, TV-minimization is reconstruction by solving an optimization problem suggested in the compressive sensing (CS) community for taking advantage of sparsity of the subject's gradient magnitude [5,6]. Various algorithms based on TV-minimization have been investigated for sparse-view CT data [7]–[13], but we have also recently begun investigating TV-minimization for many-view CT with a low X-ray intensity. While the emphasis in many of these works has been algorithm efficiency, the aim here is different in that we seek accurate solution to TV-minimization in order to simplify the trade-off study. With accurate solution of

TV-minimization, the resulting image can be regarded as a function of only the parameters of the optimization problem, removing the additional variability inherent in inaccurate but efficient TV-minimization solvers. The actual solver used here employs an accelerated gradient-descent algorithm which is described in an accompanying abstract and in Ref. [14,15]. This solver allows us to investigate the behavior of the solution to constrained, TV-minimization as the number of projections is varied at fixed total flux. As this is a preliminary study, the evaluation is based upon visual inspection of images obtained with a realistic computer-phantom and a CT data model incorporating physics of the low-intensity scan. Section II describes the system and subject model in detail; Sec. III briefly describes the reconstruction algorithm; and Sec. IV presents indicative results of the sampling/noise trade-off study for breast CT.

II. BREAST CT MODEL

We model the salient features of a low intensity X-ray CT system and a breast subject to gain an understanding of the trade-off between noise-per-projection and number-of-projections.

A. phantom

The breast phantom has four components: skin, fat, fibro-glandular tissue and micro-calcifications. The latter two components are the most relevant and are now described in detail. We refer all gray values to that of fat, which is taken to be 1.0. The skin gray level is set to 1.15.

Fibro-glandular tissue: The gray value is set to 1.1. The pattern of this tissue is generated by a power law noise model described in Ref. [16]. The complexity of this tissue's attenuation map is similar to what one could find in a breast CT slice. For the present study, the background fibro-glandular tissue, fat and skin are represented with as a 1024x1024 digital phantom, from which projections are computed. The reason for doing so, is that we want to isolate the issue of structural complexity of the background, while removing potential ambiguity of projection model mismatch.

Micro-calcifications: 5 small ellipses with attenuation values ranging from 1.8 to 2.1. In this case, the ellipse projections are generated from a continuous ellipse model, and unlike the rest of the phantom, these projections are not consistent with the digital projection system matrix. For these structures, object pixelization is a highly unrealistic model because of their small size; hence we employ the continuous model to generate their projection data.

The complete phantom along with a blow-up of a region of interest (ROI) containing the micro-calcifications is shown in Fig. 1. The complexity of background is apparent, and although the phantom is indeed piece-wise constant, the gradient magnitude has 55,000 non-zero values due to the structure complexity. This number is relevant for the CS argument on the accuracy of TV-minimization. While there has been no

¹Technical University of Denmark, Department of Informatics and Mathematical Modeling, Richard Petersens Plads, Building 321, 2800 Kgs. Lyngby, Denmark. ²The University of Chicago, Department of Radiology MC-2026, 5841 S. Maryland Avenue, Chicago IL, 60637. Corresponding author: Emil Y. Sidky, E-mail: sidky@uchicago.edu

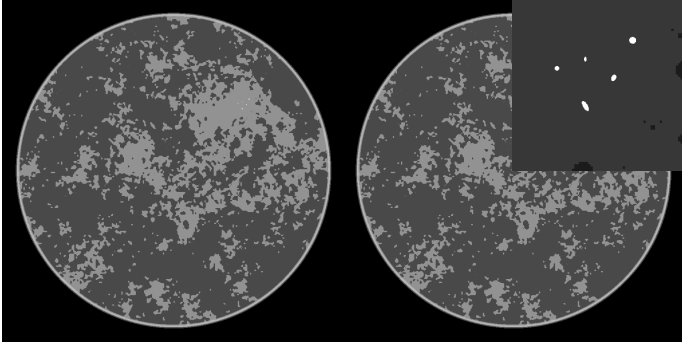


Fig. 1. Left: complete breast phantom shown in a gray scale window [0.9, 1.25]. Right: same phantom with a blown-up inset of 7.5x7.5 mm² ROI containing the micro-calcifications. The ROI grayscale window is [0.9, 1.8]. All image reconstruction results are shown in this format.

analysis of CS recovery for CT-based system matrices, one can expect that at least twice as many samples as non-zero elements in the gradient magnitude will be needed for accurate image reconstruction with TV-minimization under noiseless conditions.

B. data model

As the primary goal of this study is to investigate a noise trade-off, the CT model includes a random component modeling the detection of finite numbers of X-ray quanta. The process of generating the simulated CT data starts with computing a noiseless sinogram:

$$g_j = \int_{L_j} d\ell f_{\text{digital}}[\vec{r}(\ell)] + f_{\text{u\text{calc}}}[\vec{r}(\ell)], \quad (1)$$

where g_j is the j th line integral of the phantom over the ray L_j with the index j running from 1 to N_{data} ; N_{data} is the product of the number of projections and the number of detector bins per projection; and $f_{\text{digital}}[\vec{r}(\ell)]$ and $f_{\text{u\text{calc}}}[\vec{r}(\ell)]$ represent the digital and continuous components of the phantom, respectively. The measurements g_j are used for the noiseless reconstructions.

In order to include a random element to the data, which depends on N_{data} in a fairly realistic way, we compute a mean photon number per detector bin based on g_j and a total photon intensity of the scan:

$$n_j^{(\text{mean})} = \frac{N_{\text{photon}}}{N_{\text{data}}} \exp(-g_j),$$

where N_{photon} is the total number of photons in the scan and is here selected to be a value typical of mammography. Note that the model the scale factor will cause the mean number of photons per bin to decrease as the number of ray measurements increases. From $n_j^{(\text{mean})}$, a realization \mathbf{n}_j is selected from a Gaussian distribution, using $n_j^{(\text{mean})}$ as the mean and variance. This Gaussian distribution closely models a Poisson distribution for large $n_j^{(\text{mean})}$. Finally, the photon number noise realization is converted back to a realization of a set of line integrals:

$$\mathbf{g}_j = -\ln \left(\frac{N_{\text{data}}}{N_{\text{photon}}} \mathbf{n}_j \right).$$

It is this data set which will be used for the noisy reconstructions below. While this model incorporates the basic idea of the noise-level trade-off, there are still limitations of the study. The incident intensity on each detector bin is assumed to be the same; no correlation with neighboring bins is considered;

electronic noise in the detector is not accounted for; and reconstructions are performed from a single realization as opposed to an ensemble of realizations.

III. IMAGE RECONSTRUCTION BY CONSTRAINED TV-MINIMIZATION

In order to perform the image reconstruction, we employ CS-motivated, constrained, TV-minimization:

$$\vec{f}^* = \text{argmin} \|\vec{f}\|_{\text{TV}} \text{ subject to } |X\vec{f} - \vec{g}|^2 \leq \epsilon^2 \text{ and } \vec{f} \geq 0, \quad (2)$$

where the norm $\|\cdot\|_{\text{TV}}$ is the sum over the gradient magnitude of the image; the system matrix X represents discrete projection converting the image estimate \vec{f} to a projection estimate \vec{g} ; ϵ is a data error tolerance parameter controlling how closely the image estimate is constrained to agree with the available data; and the last constraint enforces non-negativity of the image. This optimization problem has served to aid in designing many new image reconstruction algorithms for CT. As the CT application is quite challenging, most of these algorithms do not yield the solution $\vec{f}^*(\epsilon)$ of Eq. (2), which should only depend on ϵ once the CT system parameters are fixed. As a result, these algorithms yield images which also depend on algorithm parameters. This is not necessarily a bad thing, but it becomes difficult to survey the effectiveness of Eq. (2) for various CT applications.

In applied mathematics, motivated by CS, there has been much effort in developing accurate solvers to Eq. (2), but few of these solvers can be applied to systems as large as those encountered in CT. To address this issue, we have been investigating means of accelerating gradient methods, which can be implemented for systems on the scale typical of CT. The proposed set of algorithms are described in detail in an accompanying submission to the meeting [15]. We do not discuss the algorithm here, but we point out that the optimization problem solved is modified, but equivalent to Eq. (2):

$$\vec{f}^* = \text{argmin} \alpha \|\vec{f}\|_{\text{TV}} + |X\vec{f} - \vec{g}|^2 \text{ subject to } \vec{f} \geq 0, \quad (3)$$

where the data error term has been included in the objective function, leaving only positivity as a constraint. The penalty parameter α replaces the role of ϵ above. We use the accelerated gradient algorithm to solve Eq. (3) to a numerical accuracy greater than what would be visible in the images; thus, we describe the following resulting images as solutions to this optimization problem. To make the connection with the Eq. (2) is straight-forward; the corresponding ϵ to a given α is found by computing $|X\vec{f}^* - \vec{g}|$ where \vec{f}^* is found from Eq. (3).

IV. RESULTS

For this initial survey of a breast CT simulation, we show two main sets of results. The first set of images are reconstructed from noiseless data for different numbers of views. The idea is to see how well TV-minimization performs in recovering the complex breast phantom under ideal conditions. The second set of images includes noise at a fixed exposure, and as described in Sec. II-B, the noise-level per projection increases with the the number of projections.

All reconstructions are performed on a 1024x1024 grid with 100 micron pixel widths. The simulated fan-beam geometry has an 80 cm source to detector distance with a circular source

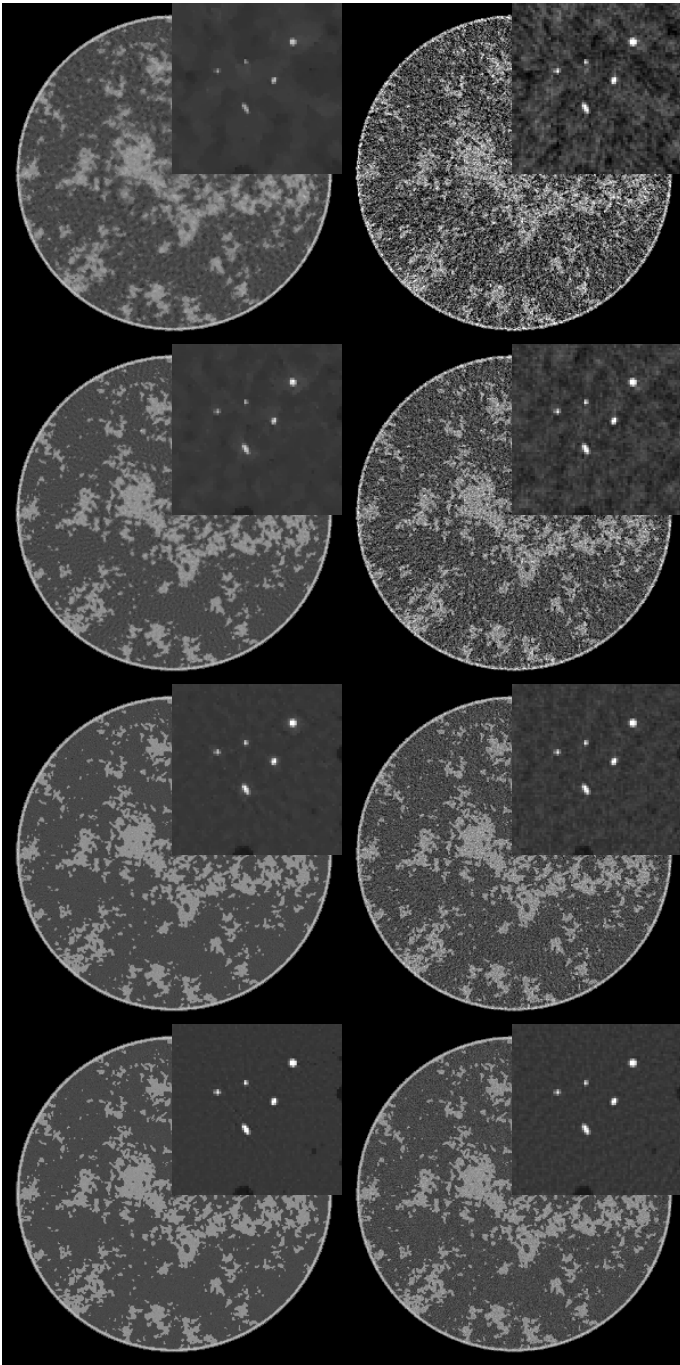


Fig. 2. Left column: images reconstructed by TV-minimization. Right column: images reconstructed by FBP. The data do not include noise, and the number of views are 64, 128, 256, and 512 going from top to bottom.

trajectory of radius 60 cm. The detector is modeled as having 1024 detector bins, and there is no truncation in the projection data.

A. image reconstruction from noiseless data

In Fig. 2, we show images reconstructed from 64 to 512 projections for both TV-minimization and filtered back-projection (FBP). For TV-minimization in this study we set $\alpha = 10^{-6}$, which corresponds to a very tight data constraint. As noted above the sparsity of the gradient magnitude is on the order of 50,000. Accordingly, from CS-based arguments, one could only expect to start to achieve accurate reconstruction when the number of measured line integrals exceeds 100,000, which in this case means 100 projections. An important part of CS theory deals with computing the factor between the sparsity

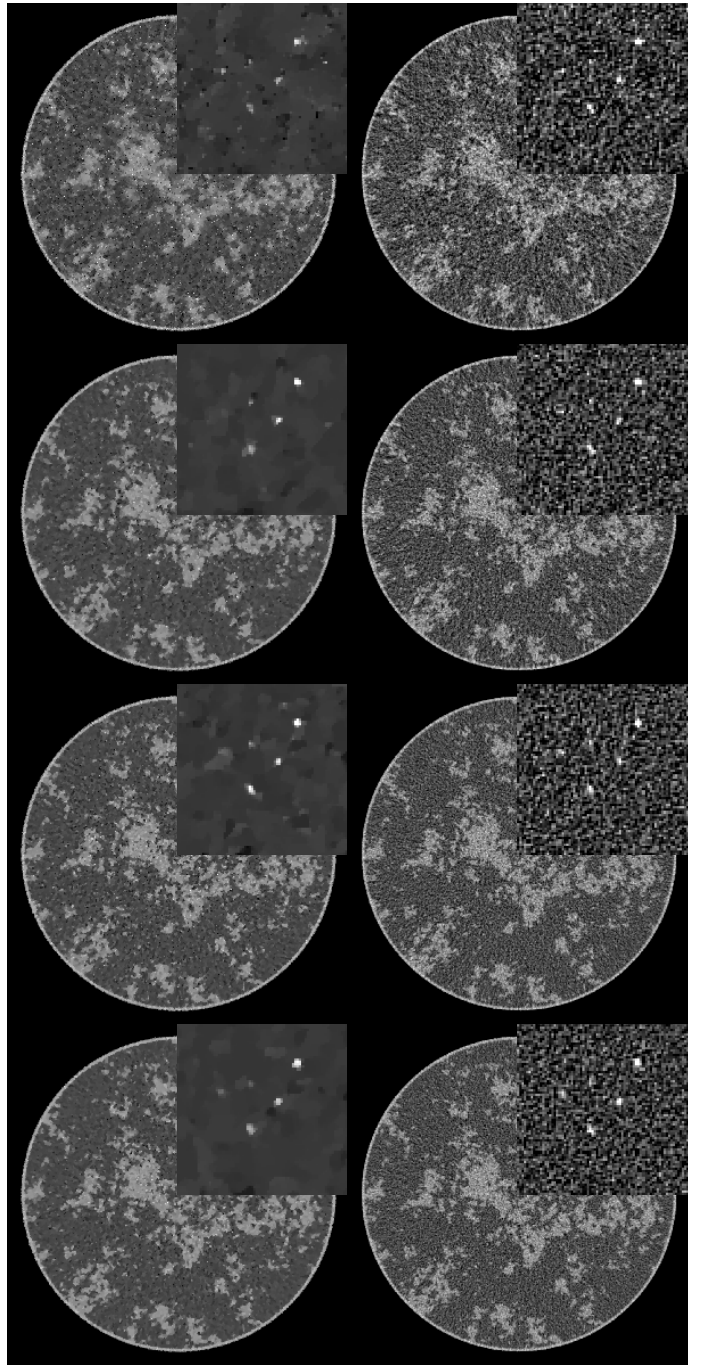


Fig. 3. Same as Fig. 2 except the noise model discussed in Sec. II-B is included.

level and necessary number of measurements for accurate recovery. This factor is unknown for TV-minimization applied to the X-ray transform, but we can see from the reconstructions that the accuracy is greatly improved in going from 128 views to 256 views. There is still a perceptible improvement in the image recovery in going to 512 views, which still represents an under-determined system despite the fact that 512 views is normally not thought of as a sparse-view data set. Again, it is the complexity of the phantom which is responsible for this behavior. The accompanying FBP results give an indication on the ill-posedness of reconstruction from the various configurations with different numbers of projections.

The results for the micro-calcification ROI are interesting in that this particular feature of the image is recovered for all data sets down to the 64-projection data set. This is not too surprising because the micro-calcifications are certainly sparse

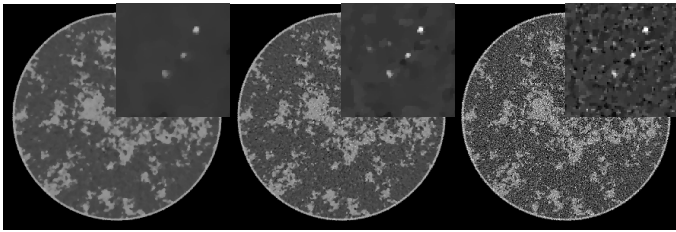


Fig. 4. Images for 512-view, noisy projection data obtained with TV-minimization for (left) $\alpha = 1 \times 10^{-3}$, (middle) $\alpha = 5 \times 10^{-4}$, and (right) $\alpha = 2 \times 10^{-4}$.

in the gradient magnitude. But this result emphasizes that the success of an image reconstruction algorithm depends also on the imaging task and the subject.

For the larger goal of determining the optimal number of views, it is clear that "structure noise" – artifacts due to the complex object function – can play a significant role for this breast phantom.

B. image reconstruction from noisy data

For the noise studies, we again investigate data sets with the view number varying between 64 and 512. For these reconstructions, α is also varied between $1. \times 10^{-6}$ and $5. \times 10^{-4}$. In Fig. 3, we show the TV-minimization images compared with FBP, as a reference. The optimal values of α for each TV-minimization image is chosen by visual inspection. The FBP fill images are smoothed by convolving with a Gaussian distribution of width 140 microns (chosen by visual inspection), and the ROI images are unregularized. While it is not too surprising that the FBP image quality appears to increase with projection number, it is somewhat surprising that the same trend is apparent for image reconstruction by TV-minimization. The 512-view data set seems to yield, visually, the optimal result in that the ROI appears to have the least amount of artifacts. While most of the micro-calcifications are visible in each reconstruction, the artifacts and noise texture in the sparse-view images can be distracting and mistaken for additional micro-calcifications. It seems that the increased noise-level per view impacts the reconstruction less than artifacts due to insufficient sampling. That we obtain this result with a CS algorithm is interesting, and warrants further investigation with more rigorous and quantitative evaluation.

To appreciate the impact of α , we focus on the 512-view data set and display images in Fig. 4 for three cases. Small α corresponds to a tight data constraint, resulting in salt-and-pepper noise in the image due to the high noise-level of the data. Increasing α reduces the image noise and eventually removes small structures.

V. CONCLUSION

We have performed a preliminary investigation of a fixed X-ray exposure trade-off between number-of-views and noise-level per view for a simulation of a breast CT system. This investigation employed a CS image reconstruction algorithm which should favor sparse-view data. Moreover, the simulated data are generated from a digital projection matched with the projector used in the image reconstruction algorithm – another factor that should favor sparse-view data. Despite this, the complexity of the subject overrides these points and it appears that the largest number of views, in the study, yields visually the optimal reconstructed images. When other physical factors are included in the data model, for example, partial volume

averaging and X-ray beam polychromaticity, one can expect that this same conclusion will hold.

Extensions to the image reconstruction algorithm will address better noise modeling. One can expect an improvement in image quality by employing a weighted, quadratic data error term derived from a realistic CT noise model. As for CS-motivated image reconstruction, the breast CT system may benefit from exploiting other forms of sparsity.

VI. ACKNOWLEDGMENTS

This work is part of the project CSI: Computational Science in Imaging, supported by grant 274-07-0065 from the Danish Research Council for Technology and Production Sciences. E.Y.S. and X.P. were supported in part by NIH R01 Grant Nos. CA120540 and EB000225. I.S.R. was supported in part by NIH Grant Nos. R33 CA109963 and R21 EB8801. The contents of this article are solely the responsibility of the authors and do not necessarily represent the official views of the National Institutes of Health.

REFERENCES

- [1] C. H. McCollough, A. N. Primak, N. Braun, J. Kofler, L. Yu, and J. Christner, "Strategies for reducing radiation dose in ct," *Radiol. Clin. N. Am.*, vol. 47, pp. 27–40, 2009.
- [2] B. Chen and R. Ning, "Cone-beam volume CT breast imaging: Feasibility study," *Med. Phys.*, vol. 29, pp. 755–770, 2002.
- [3] A. L. C. Kwan, J. M. Boone, K. Yang, and S. Y. Huang, "Evaluation of the spatial resolution characteristics of a cone-beam breast CT scanner," *Med. Phys.*, vol. 34, pp. 275–281, 2007.
- [4] C. J. Lai, C. C. Shaw, L. Chen, M. C. Altunbas, X. Liu, T. Han, T. Wang, W. T. Yang, G. J. Whitman, and S. J. Tu, "Visibility of microcalcification in cone beam breast CT: Effects of x-ray tube voltage and radiation dose," *Med. Phys.*, vol. 34, pp. 2995–3004, 2007.
- [5] E. J. Candès, J. Romberg, and T. Tao, "Robust uncertainty principles: Exact signal reconstruction from highly incomplete frequency information," *IEEE Trans. Inf. Theory*, vol. 52, pp. 489–509, 2006.
- [6] E. J. Candès and M. B. Wakin, "An introduction to compressive sampling," *IEEE Signal Process. Mag.*, vol. 25, pp. 21–30, 2008.
- [7] E. Y. Sidky, C.-M. Kao, and X. Pan, "Accurate image reconstruction from few-views and limited-angle data in divergent-beam CT," *J. X-ray Sci. Tech.*, vol. 14, pp. 119–139, 2006.
- [8] J. Song, Q. H. Liu, G. A. Johnson, and C. T. Badea, "Sparseness prior based iterative image reconstruction for retrospectively gated cardiac micro-CT," *Med. Phys.*, vol. 34, pp. 4476–4483, 2007.
- [9] G. H. Chen, J. Tang, and S. Leng, "Prior image constrained compressed sensing (PICCS): a method to accurately reconstruct dynamic CT images from highly undersampled projection data sets," *Med. Phys.*, vol. 35, pp. 660–663, 2008.
- [10] E. Y. Sidky and X. Pan, "Image reconstruction in circular cone-beam computed tomography by constrained, total-variation minimization," *Phys. Med. Biol.*, vol. 53, pp. 4777–4807, 2008.
- [11] F. Bergner, T. Berkus, M. Oelhafen, P. Kunz, T. Pan, R. Grimmer, L. Ritschl, and M. Kachelriess, "An investigation of 4D cone-beam CT algorithms for slowly rotating scanners," *Med. Phys.*, vol. 37, pp. 5044–5054, 2010.
- [12] K. Choi, J. Wang, L. Zhu, T.-S. Suh, S. Boyd, and L. Xing, "Compressed sensing based cone-beam computed tomography reconstruction with a first-order method," *Med. Phys.*, vol. 37, pp. 5113–5125, 2010.
- [13] J. Bian, J. H. Siewerdsen, X. Han, E. Y. Sidky, J. L. Prince, C. A. Pelizzari, and X. Pan, "Evaluation of sparse-view reconstruction from flat-panel-detector cone-beam CT," *Phys. Med. Biol.*, vol. 55, pp. 6575–6599, 2010.
- [14] T. L. Jensen, J. H. Jørgensen, P. C. Hansen, and S. H. Jensen, "Implementation of an optimal first-order method for strongly convex total variation regularization," *submitted*.
- [15] J. H. Jørgensen, T. L. Jensen, P. C. Hansen, S. H. Jensen, E. Y. Sidky, and X. Pan, "Accelerated gradient methods for total-variation-based ct image reconstruction," in *submitted to the 2011 International Meeting on Fully Three-Dimensional Image Reconstruction in Radiology and Nuclear Medicine*, Potsdam, Germany, 2011.
- [16] I. Reiser and R. M. Nishikawa, "Task-based assessment of breast tomosynthesis: Effect of acquisition parameters and quantum noise," *Med. Phys.*, vol. 37, pp. 1591–1600, 2010.